Performance analysis of the vehicle electronic stability control in emergency maneuvers at low-adhesion surfaces

Performance analysis of the vehicle electronic stability control in emergency maneuvers at low-adhesion surfaces

I Kulikov[1] **and J Bickel**[2]

[1] Department of Powertrains, Federal State Unitary Enterprise "NAMI", Moscow, Russian Federation
[2] Faculty of Engineering and Computer Science, University of Applied Sciences "Hochschule Osnabrück", Osnabrück, Germany

Email: i.kulikov.mami@gmail.com

Abstract
Essential principles of the vehicle electronic stability control (ESC) operation are analyzed. Mathematical model employed for the performance investigation of vehicles equipped with ESC is described. Modeling results are presented, simulating the actual road test, in which ESC-equipped vehicle performed an emergency maneuver at the surface covered with packed snow. Modeling allowed identifying ESC interventions occurred in the road test. Also, modeling results are presented, simulating the same road test with disabled ESC and with replacement of the original ESC by an experimental yaw stability controller. Conclusions are drawn about performance of both original ESC and the experimental controller. Analysis of the simulation results allowed disclosing changes of the vehicle steering behavior during the maneuver, as well as stability loss factors emerging at particular points of the maneuver. Variation of controller's parameters allowed defining conditions in which ESC should intervene to prevent the vehicle from a skid.

1. Introduction

Vehicle emergency handling constitutes an example of transient maneuvers with a substantial risk of losing directional stability. This may take place during a sharp lane changing in order to avoid collision with a sudden obstacle. At low-adhesion surfaces, such maneuvers become especially unsafe.

At present, performance of vehicle electronic stability control systems at low adhesion surfaces can be considered as an insufficiently investigated issue. Global Technical Regulation No. 8 (GTR 8) is entirely dedicated to the ESC and includes a substantial analytical section; however, while stating the importance of said issue, this Regulation nevertheless offers neither analysis nor testing procedures for ESC operation at low adhesion surfaces. Among known literature on this problem, one can notice the works [1, 2], which describe experimental investigations of ESC performance at icy surfaces on vehicle equipped with studded tires. The experiments included "sine with dwell" maneuver specified by GTR 8. At the same time, for getting a deeper insight into vehicle dynamics at low adhesion surfaces with ESC interventions, theoretical investigations are also required. However, their number is small as well. One of the rare examples is [3] describing problem analysis and tire modeling taking into account ESC operation at slippery roads. Therefore, elimination of the research gap in this field can be considered an urgent task, which is addressed in the work described by this paper. To allow the reader better grab

approaches of this investigation, as well as its results, first sections of the paper provide descriptions of the essential principles of operation and control of ESC systems.

2. ESC basic operation principles

During transient directional motion, vehicle steering behavior changes both quantitatively and qualitatively, i.e. showing transitions between oversteering and understeering. Transient steering behavior is defined by the yawing moment. The latter is built by the sum of tire force moments exerted by individual wheels. Difference between front and rear tire forces makes that sum deviate from zero when transient directional motion takes place. On the one hand, the yawing moment constitutes an immanent feature of the transient turn. On the other hand, this moment makes rising vehicle deviation from the neutral steering behavior. With certain vehicle velocity, steering wheel angle and steering dynamics, transient process does not converge to a stable state bringing vehicle into a skid. In other cases and conditions, transient process may lead to a stable state, which nevertheless prevents vehicle from following the trajectory specified by the driver, which is called drift.

The ESC system is intended for preventing skids and drifts through altering of the vehicle yawing moment [4, 5]. By its operation principle, ESC can be called a yaw controller of extremal type, because it only intervenes into vehicle motion if there is a risk of stability loss. ESC corrects vehicle steering behavior by regulation of yawing moments created by the individual wheels. This is achieved by altering tire force magnitude, or tire force arm, or both. These corrections are implemented through the known tire-surface adhesion property, i.e. association between longitudinal and lateral adhesion coefficients. The simplest model of this property is the Kamm's circle. It shows the relation between the tire force vector direction and the tire slip in both longitudinal and lateral directions: changes in these slip components cause rotation of the tire force vector. In figure 1, the tire force vector R_{12} at the front left wheel rotates from the initial position ($R_{12,i}$) into the final position ($R_{12,f}$). This rotation changes the tire force arm from $h_{12,i}$ to $h_{12,f}$. Assuming the vector magnitude constant, the change in yawing moment reads $\Delta M_z = R_{12} \cdot (h_{12,i} - (-h_{12,f}))$. Figure 1 shows a vehicle performing right turn, in which the front left tire creates the largest yawing moment increasing oversteering and, possibly, leading into a skid. Rotating this tire force vector clockwise, as it is shown in figure 1, diminishes oversteering behavior, thus preventing vehicle from a skid.

Since tire sideslip depends on directional motion dynamics, which is defined by the vehicle velocity, the steering wheel angle, and steering dynamics (in other words, defined by the driver and driving conditions), it cannot be employed for the controllable change of the tire force vector. This change can only be performed by the longitudinal tire slip control, which is achieved through the regulation of the wheel torque (T_w). The latter is provided by the engine (altered by the transmission) and brakes. Automatic control of these components, allowing regulation of torques at individual wheels, implements the slip control, and thus provides tire force rotation feature. This mechanism is essential for the ESC operation.

Backward rotation of the tire force vector at the front outer wheel (with respect to the center of the turn) constitutes the main operation performed by the ESC. This operation is relatively simple to implement – by means of a brake mechanism – and creates unambiguous effect: both decreasing of R_y component and increasing of $-R_x$ component diminish the yawing moment, which leads into a skid. Note that decreasing of the R_y requires a substantial longitudinal slip to be attained, which implies bringing tire beyond the maximum point of its adhesion characteristic (since this is the only way to rotate the tire force vector at a large enough angle). Additionally, ESC can operate at the rear outer wheel. It also should be braked, however, braking torque should have the magnitude that allows increasing $-R_x$ component, which acts against skid, without decreasing R_y component, which also counteracts skid. To meet this requirement, tire should be operated below its adhesion maximum, preventing the lateral force from falling. ESC operation at inner wheels is a more contradictory and complicated option, because: it requires creating non-symmetrical traction torques (which is technically more difficult than braking), produces rather ambiguous effect (increasing the vehicle speed and, as a

result, the lateral acceleration), and is less effective in the sense of yawing moment correction (because the tire force is relatively small due to decreased weight acting on inner wheels).

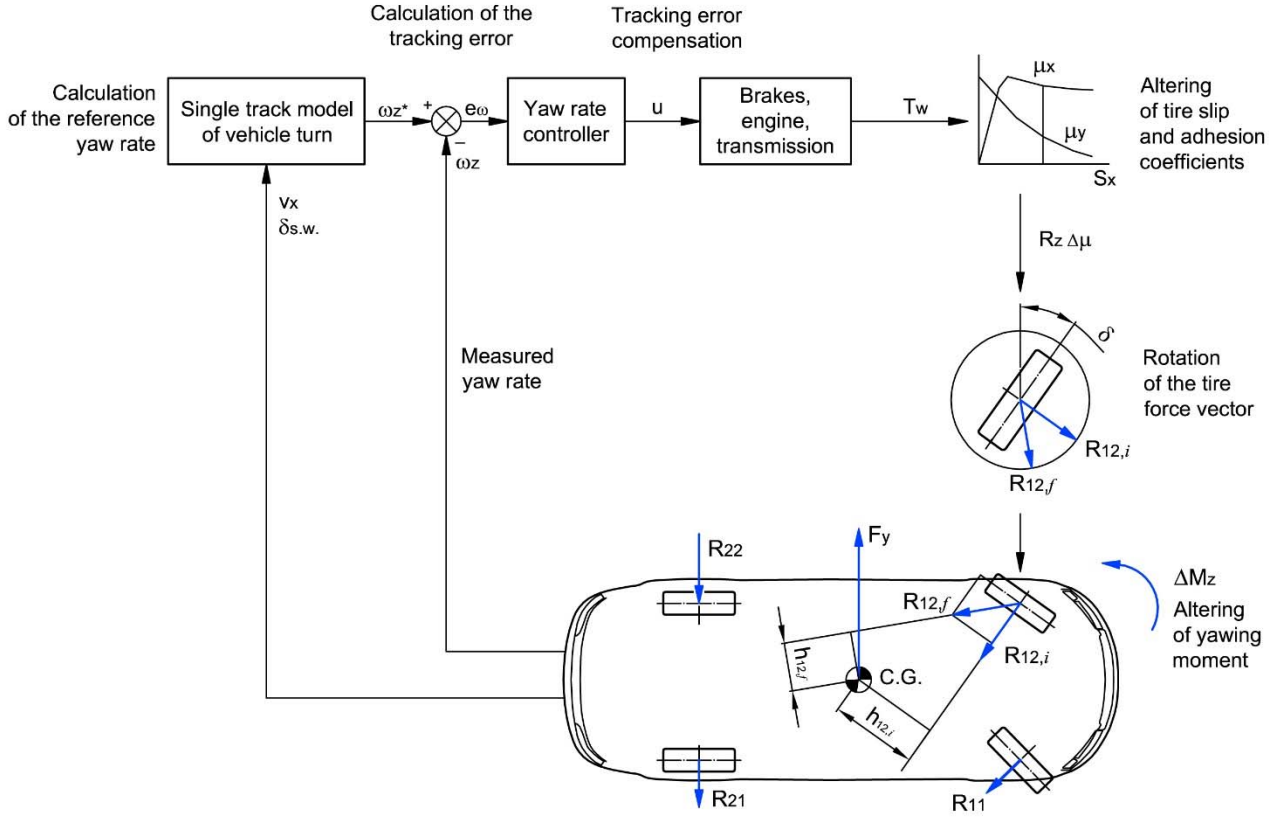

Figure 1. Vehicle electronic stability system operation and control loop.

3. ESC control

The ESC is a feedback yawing moment controller (see figure 1 for the control loop). The main components of such a system are the regulator generating control signal, the command signal for controlled variable, and the feedback signal. In the ESC, controlled variable is the yaw rate. This variable is involved as the basic parameter in a number of vehicle handling characteristics [6], being a sufficient quantitative measure of the vehicle steering behavior. Reference steering behavior of the vehicle can be defined by calculation of the corresponding yaw rate. The simplest way for calculating this reference yaw rate is to employ the single-track kinematic model of the vehicle turn (figure 2).

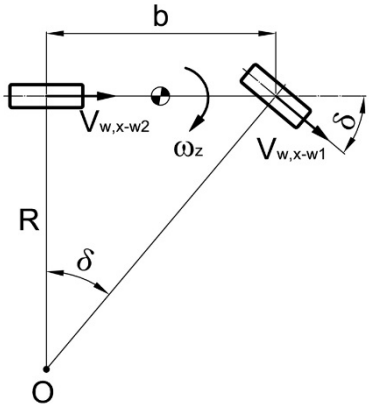

Figure 2. Single-track kinematic model of the vehicle turn on rigid wheels.

From this figure, an expression for the yaw rate can be derived, which depends on small number of parameters (see nomenclature of variables and parameters in the appendix):

$$\omega_z = \frac{V_{w-x,w2} \cdot \delta_{s.w.} \cdot u_{steer}}{b} \quad (1)$$

All these parameters can be determined in the ESC controller with sufficient precision, including vehicle velocity, although usually it does not coincide with the wheel linear velocity due to slip, which implies some sort of observer to be utilized to calculate it.

Yaw rate calculated by equation (1) corresponds to the Ackermann's kinematics, since there are no sideslip angles in this model. To make this model providing desired characteristics of understeering or oversteering, it is augmented with certain modifications [5]. One of them adds the cornering stiffness of tires. It must be noted that cornering stiffness coefficients depend on tire-surface adhesion, which should be identified by ESC controller in real-time. Second modification adds a dead zone at the input of the yawing moment regulator to adjust its sensitivity to the deviation between the actual yaw rate and the required one. Having that deviation within limits of the dead zone will prevent the ESC regulator from undesirable interventions into vehicle motion. Yet another modification is introduced to address difference between the steady state turn calculated by the model (1) and actual dynamics of the vehicle directional motion. This modification implies passing the calculated yaw rate signal through a filter having time constant, which corresponds to vehicle inertial properties. All mentioned modifications allow defining thresholds between save maneuvering, intervention to which is not necessary and negatively perceived by drivers, and critical maneuvering, which requires ESC interventions.

In addition, calculated yaw rate should be limited by the maximum lateral tire adhesion [5], which is defined for the steady-state single-track model as follows:

$$a_y = \frac{V_{w,x-w2}^2}{R} = \omega_z \cdot V_{w,x-w2} \leq \mu_{y,max} \cdot g \;\rightarrow\; \omega_z \leq \frac{\mu_{y,max} \cdot g}{V_{w,x-w2}}$$

Maximum lateral adhesion coefficient should be identified by indirect methods. Accuracy of this identification influences ESC performance at a given road surface.

The feedback signal of the ESC regulator is the actual yaw rate measured onboard by a gyroscopic sensor. Difference between required and measured yaw rate is fed into the regulator input. In the sophisticated production ESC systems, the regulator outputs correcting yawing moment command, which is distributed between separate wheels by means of weighting function [5]. In turn, yawing moment assigned to each wheel is converted into the longitudinal slip, which is required for corresponding rotation of the tire force vector. This conversion is performed by means of the Kamm's circle and the following variables calculated by the controller: wheel normal force, maximum tire-surface adhesion coefficient, and sideslip angle. The slip command is compared to the actual slip, which is also obtained by means of calculations. Resulting slip difference is fed into low-level controllers, which implement required slip by providing appropriate torques by brakes, engine, and transmission.

Production ESC systems employ yaw rate controllers in the form of PID regulators with variable gains [5], which depend on the vehicle velocity and the tire-road adhesion. Additionally, the proportional gain constitutes a non-linear function of the calculated vehicle sideslip angle.

Performance of an ESC system having control signals defined by indirect calculations of unmeasured quantities (so called virtual sensors) depends on accuracy of employed models, which is obviously limited and can deteriorate in complicated operating conditions like unsteady road adhesion, tire wearing, and so on. For compensation of inaccuracy or/and disturbances, ESC can use some methods of adaptive control. In the literature, different ways of implementing such systems are proposed – from employing of auxiliary relay regulators [7], to fuzzy logic [8], and artificial neural networks [9].

One can notice that existing literature on ESC systems mostly focuses on control systems and methods [7-10] paying much less attention to the controlled object, i.e. the vehicle. In many works, vehicle is treated as a "black box" modeled by library-based software such as ADAMS Car or CarSim. Such works show an approach involving analysis of two or three basic quantities (lateral acceleration,

yaw rate, and body roll angle) of the vehicle directional motion, which only allows stating that ESC has prevented or has not prevented the loss of stability; however this approach does not answer the question "why did that happen"?

Research and development of the ESC should be conducted along with thorough analysis of vehicle handling properties. It is necessary to study conditions and factors of stability loss, as well as mechanisms of its prevention by the ESC. In particular, it should be investigated at which stage of a handling maneuver the ESC has to intervene to maintain vehicle stability. This paper describes results of the research, which was aimed at addressing these issues. The main tools of this research were the mathematical model described in the next section and the results of road tests performed on ESC-equipped vehicle. For implementation of the vehicle stability control feature, a relatively simple yaw rate regulator was elaborated, which only outputs torque command for the front outer wheel, which yawing moment is the major factor of skid prevention. During the investigation, regulator adjustments were varied in order to disclose their effect on the vehicle handling ability.

4. Model of vehicle dynamics

In this work, vehicle was modelled as a multibody system comprising six masses: vehicle itself performing a planar motion, the sprung mass moving in lateral plane (body roll), and four rotating masses of the wheels. Wheel normal forces were calculated based on force equilibrium in both longitudinal and lateral planes. Neglecting a small angular speed of the sprung mass around the lateral axis allowed excluding association between angular speeds and accelerations from the Euler dynamic equations. Products of inertia, also assumed negligible, were excluded from the equations of vehicle motion and body roll.

Figure 3 shows schematics used to derive the equations of vehicle dynamics.

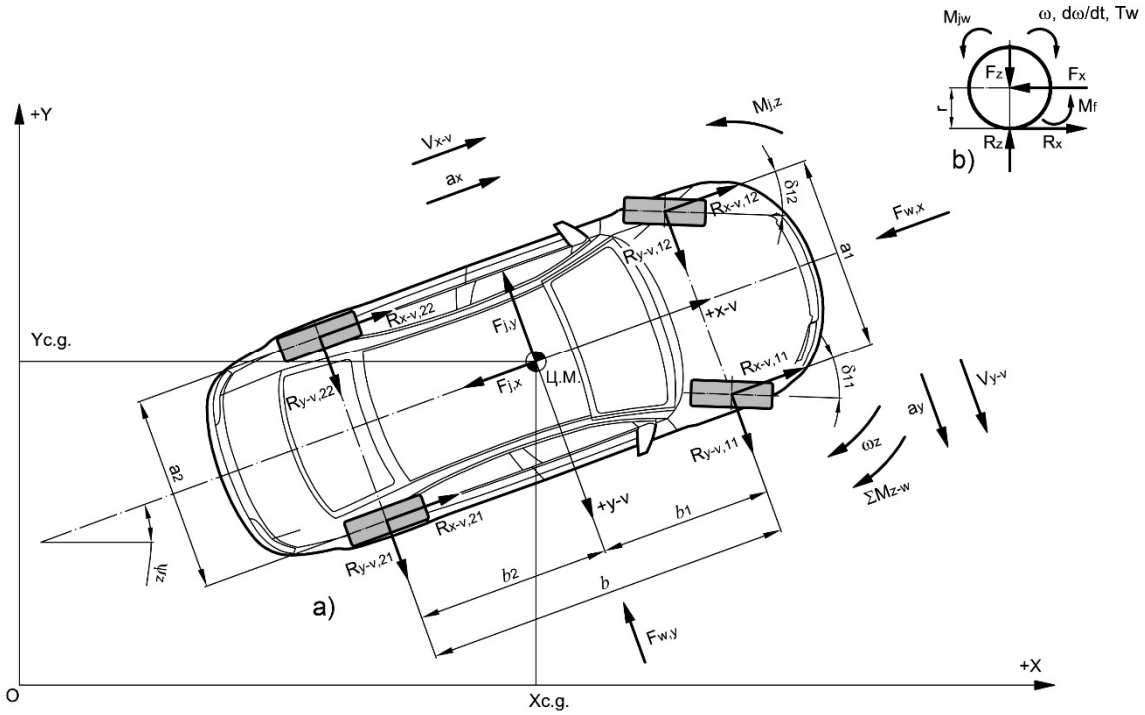

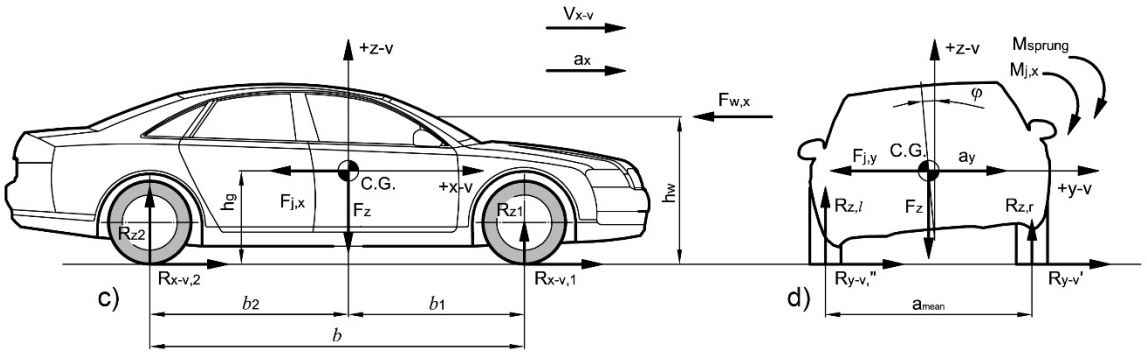

Figure 3. Schematics for the vehicle dynamics model. a – vehicle planar motion; b – wheel rotational dynamics; c – calculation of the tire normal forces in longitudinal plane; d – body roll and tire normal forces in lateral plane.

The following coordinate systems were implemented within the model: associated with the road plane, associated with the vehicle (corresponding variables are denoted by "v" index), and associated with each wheel (corresponding variables are denoted by "w" index). Also, designations of variables and parameters associated with the wheels include indices *ij*, where *i* denotes axis number, and *j* denotes wheel number associated with *i*-th axis.

The equation system derived from these schematics and assumptions, reads as follows (see nomenclature of variables and parameters in the end of the paper):

$$\begin{cases} m \cdot a_{x,c.g.} = m \cdot \left(\dot{V}_{c.g.,x-v} - \omega_z \cdot V_{c.g.,y-v}\right) = \sum_{i=1}^{n}\sum_{j=1}^{k} R_{x-v.ij} - F_{w,x} \\ m \cdot a_{y,c.g.} = m \cdot \left(\dot{V}_{c.g.,y-v} + \omega_z \cdot V_{c.g.,x-v}\right) = \sum_{i=1}^{n}\sum_{j=1}^{k} R_{y-v.ij} - F_{w,y} \\ \mathcal{J}_z \cdot \ddot{\psi}_z = \mathcal{J}_z \cdot \dot{\omega}_z = \sum_{i=1}^{n}\sum_{j=1}^{k} M_{z-v.ij} \\ \mathcal{J}_{x,sprung} \cdot \ddot{\varphi} = \sum_{i=1}^{n}\sum_{j=1}^{k}\left(R_{y-v.ij} \cdot h_{c.g.}\right) - \varphi \sum_{i=1}^{n} c_{\varphi i} - \dot{\varphi} \sum_{i=1}^{n} d_{\varphi i} \\ \mathcal{J}_{w,ij} \cdot \dot{\omega}_{w,ij} = T_{w,ij} - \left(R_{z,ij} \cdot f_{ij} + R_{x-w.ij}\right) \cdot r_{ij} \end{cases} \quad (2)$$

5. Model of vehicle kinematics

Tire force vector components included in the system (2) constitute functions of tire longitudinal slip and sideslip angles. For calculation of these parameters, a kinematic model of the vehicle was employed considering vehicle as a body performing a planar motion. With this assumption, the velocity graph of vehicle was drawn; figure 4 shows a part of this graph corresponding to the front left wheel.

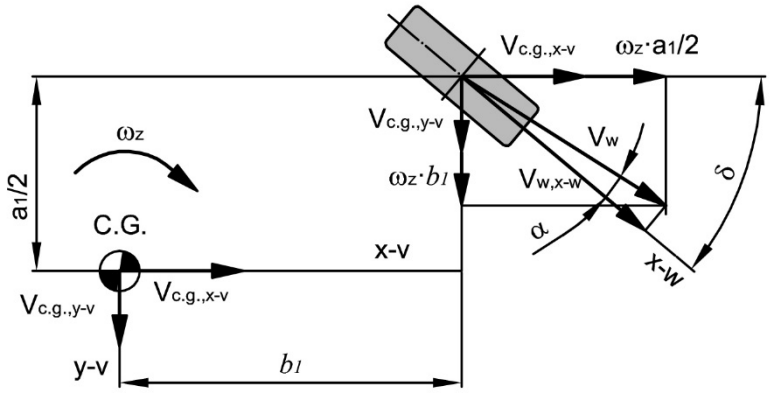

Figure 4. Velocity graph for the vehicle kinematic model.

Baseline point of this graph is the vehicle center of gravity (C.G.), which linear velocity components ($V_{c.g.,x-v}$, $V_{c.g.,y-v}$), as well as the vehicle yaw rate, are calculated by the model of vehicle dynamics (2). With these quantities, projections of the wheel linear velocity on the vehicle axes are calculated as follows:

$$V_{w,x-v,ij} = V_{c.g,x-v} \pm \omega_z \cdot \frac{a_i}{2}$$

$$V_{w,y-v,ij} = V_{c.g,y-v} \pm \omega_z \cdot b_i + \frac{\partial y_{w-v,ij}}{\partial \varphi}\dot{\varphi}$$

For "x-v" axis projection, the second term is taken with "+" for the right wheels. For "x-y" axis projection, the second term is taken with "+" for the front wheels. Lateral velocity component $V_{w,y-v,ij}$ is calculated taking into account lateral displacement of the wheel resulting from the body roll. This is accomplished by employing derivative $\frac{\partial y_{w-v,ij}}{\partial \varphi}$, which constitutes a kinematic characteristic of the suspension [6, 11].

Sideslip angle is calculated as follows:

$$\alpha_{ij} = arctan\left(\frac{V_{w,y-v,ij}}{V_{w,x-v,ij}}\right) - \left(\delta_{ij} + \frac{\partial \delta_{ij}}{\partial \varphi}\varphi\right).$$

Besides the wheel steer angle δ_{ij} resulted from the steering wheel rotation, this equation takes into account additional angle resulted from the body roll and calculated by another kinematic characteristic of the suspension $\frac{\partial \delta_{ij}}{\partial \varphi}$, which introduces relation between the body roll and the toe-in angle of the wheel [6, 11].

The full vector of the wheel center linear velocity is defined by its components:

$$V_{w,ij} = \sqrt{V_{w,x-v,ij}^2 + V_{w,y-v,ij}^2}$$

Projecting the wheel center velocity $V_{w,ij}$ on the wheel longitudinal plane and dividing it by the wheel angular velocity yields the wheel rolling radius:

$$r_{e,ij} = \frac{V_{w,ij} \cdot cos\alpha_{ij}}{\omega_{w,ij}}.$$

For calculation of the tire longitudinal slip, one of the following expressions is utilized constituting ratios between the current wheel rolling radius and the effective rolling radius $r_{e0,ij}$ for traction and braking modes of the wheel:

$$S_{x,tr.} = 1 - \frac{r_{e,ij}}{r_{e0,ij}};\ S_{x,br.} = -\left(1 - \frac{r_{e0,ij}}{r_{e,ij}}\right).$$

Effective rolling radius $r_{e0,ij}$ is determined experimentally under free rolling conditions when the vehicle is driving along a straight line.

6. Tire model

In this work, an empirical model called the Magic Formula (MF) devised by H. Pacejka [12] is employed for calculation of tire-surface adhesion characteristics. The MF model approximates both longitudinal and lateral components of the tire force vector with unified trigonometric functions:

$$R_{x-w,0} = D_x \cdot \sin\left(C_x \cdot arctan\left(B_x \cdot S_x - E_x\left(B_x \cdot S_x - arctan(B_x \cdot S_x)\right)\right)\right),$$

$$R_{y-w,0} = D_y \cdot \sin\left(C_y \cdot arctan\left(B_y \cdot \acute{\alpha} - E_y\left(B_y \cdot \acute{\alpha} - arctan\left(B_y \cdot \acute{\alpha}\right)\right)\right)\right),$$

where $\acute{\alpha} = -\alpha$ (the lateral tire force acts in opposite direction to the sideslip angle). Index "0" denotes that these equations calculate tire forces for the cases of pure longitudinal slip ($\alpha \approx 0$) and pure sideslip ($S_x \approx 0$). Combined slip is taken into account by the correcting functions described below. B, C and E coefficients are identified by means of experimental data acquired from vehicle or tire test results. D coefficient constitutes a product of the maximum longitudinal/lateral adhesion coefficient and the tire normal force: $\mu_{x/y,max} \cdot R_{z,}$.

Tire aligning moment is calculated by the following function:

$$M_{z-w} = -R_{y-w,0} \cdot D_t \cdot \cos\left(C_t \cdot arctan\left(B_t \cdot tan(\acute{\alpha}) - E_t\left(B_t \cdot tan(\acute{\alpha}) - arctg(B_t \cdot tg\acute{\alpha})\right)\right)\right).$$

Equation of the longitudinal tire force for the combined slip reads:

$$R_{x-w} = R_{x-w,0} \cdot G_{xy},$$

where $G_{xy} = \cos\left(C_{xy} \cdot arctan\left(B_{xy} \cdot tan(\acute{\alpha}) - E_{xy}\left(B_{xy} \cdot tan(\acute{\alpha}) - arctan\left(B_{xy} \cdot tg\acute{\alpha}\right)\right)\right)\right)$ is the correction function taking into account sideslip. A similar formula is applied for the correction of the lateral tire force, with the longitudinal slip S_x as an argument of the correction function.

Tire forces calculated by the MF model are projected from the wheel axes onto the vehicle axes in accordance with schematics of figure 5.

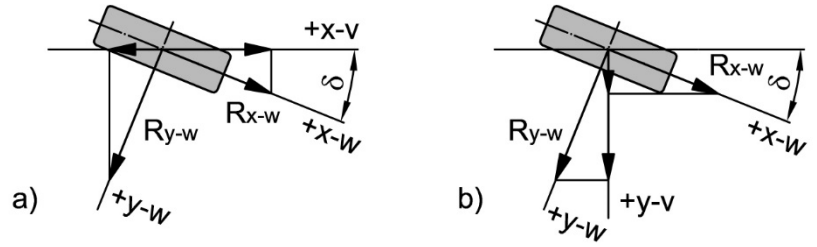

Figure 5. Projection of the tire force vector from the wheel axes onto the vehicle axes. a – on the longitudinal axis of the vehicle; b – on the lateral axis of the vehicle.

From these schematics, the following equations of longitudinal and lateral components of the tire force projected on the vehicle axes were derived:

$$\begin{cases} R_{x-v,ij} = R_{x-w,ij} \cdot cos\delta_{ij} - R_{y-w,ij} \cdot sin\delta_{ij} \\ R_{y-v,ij} = R_{x-w,ij} \cdot sin\delta_{ij} + R_{y-w,ij} \cdot cos\delta_{ij} \end{cases}$$

Using these projections and schematics shown in figure 3a allows defining yawing moment exerted by the *ij*-wheel:

$$M_{z-v,ij} = \pm R_{x-v,ij} \cdot \frac{a_i}{2} \pm R_{y-v,ij} \cdot b_i + M_{z-w,ij}.$$

According to the accepted sign convention, the moment of the longitudinal tire force is taken with "+" for the left wheels, and with "–" for the right wheels; the moment of the lateral tire force is taken with "+" for the front wheels, and with "–" for the rear wheels.

7. Experimental research

The studied vehicle was tested at the NAMI Testing Center by the Vehicle Safety Department. Physical and design parameters of the vehicle, which are essential for modeling, were determined by means of laboratory tests. In particular, vehicle weight parameters were measured, and center of gravity coordinates determined. Also, measurements were conducted, which allowed calculation of the steering mechanism characteristics. The road tests were performed at surfaces covered with packed snow and ice. The testing program consisted of both ESC-on and ESC-off emergency maneuvers (figure 6).

Figure 6. Performing of a "lane change" road test.

The employed test equipment allowed measuring the following signals: steering wheel angle, vehicle longitudinal velocity, wheel rpm, linear accelerations and angular velocities at certain points of the vehicle body. Description of the conducted tests as well as the measuring equipment can be found in [13].

8. Tire model parameters identification

Since no separate tire tests were conducted, adhesion characteristics have been identified by means of modeling. Identification implies varying MF coefficients with assessment how these affect certain variables of the vehicle dynamics (longitudinal velocity, linear accelerations, and yaw rate). Coefficient values, which provide modeling with minimum relative mean square errors (MSE) for those dynamic variables are considered acceptable. The identification procedure was organized as follows. First to be determined were characteristics of the pure tire slip. Pure longitudinal slip parameters can be determined from tests where maximum longitudinal acceleration/deceleration is achieved. This takes place in emergency braking tests. Pure sideslip takes place in tests where vehicle is steered at constant speed

achieving maximum lateral acceleration. An example of such test is emergency lane changing. Having the pure slip characteristics defined, identification of the combined slip correction functions can be performed using experiments with ESC interventions. It should be stressed that the correction functions are crucial for ESC modeling, since the operation principle of ESC is based on tire combined slip properties.

Figure 7 shows an example of identified adhesion characteristics for the surface covered with packed snow. Note that the tested vehicle was equipped with studded tires.

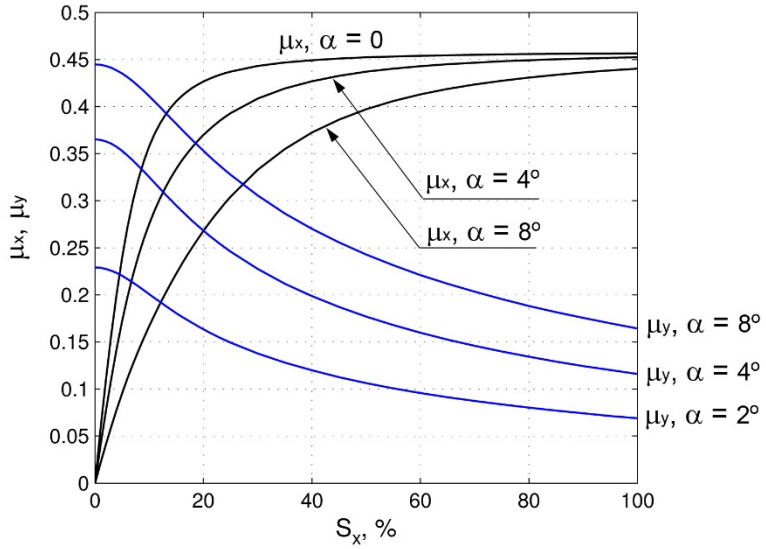

Figure 7. Identified tire adhesion characteristics for the packed snow.

9. Identification of the wheel torques

Modeling of active safety systems implies determination of the wheel torques. Since in this work these were not measured during the road tests, in the model they were calculated by means of the torque observers [13, 14]. These were implemented by the feedback control systems regulating wheel torques (figure 8). For such torque controller, the command signal is the wheel angular velocity measured during a test, and the feedback signal is the angular velocity of the same wheel calculated by the vehicle model. In order to compensate difference between the command value and the feedback value, the regulator calculates the wheel torque.

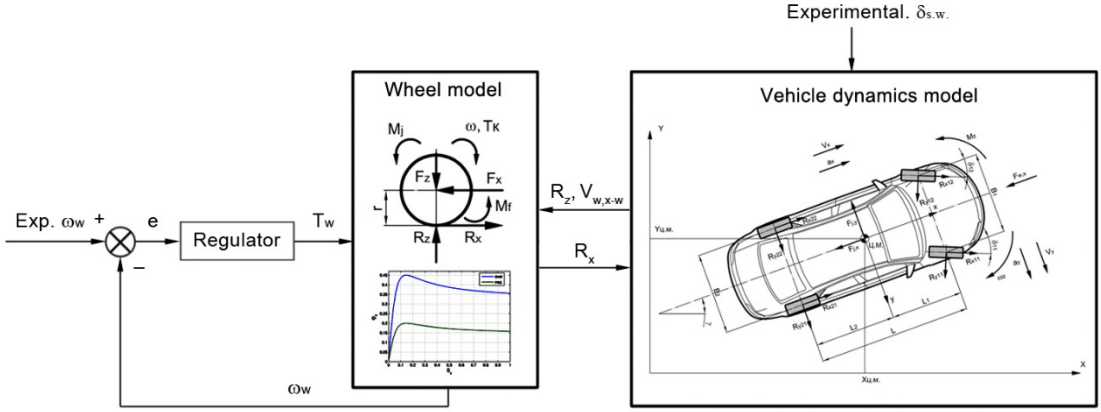

Figure 8. Identification of unmeasured wheel torques (torque observer).

Accuracy of identification depends on overall validity of the vehicle model and is evaluated indirectly, i.e. by relative mean square errors of vehicle velocity and acceleration. Another criterion is

the qualitative correspondence of the identification results to operation principles of the considered active safety system. For example, in maneuvers with an ESC system enabled, one can expect pronounced correction torques to be identified at individual wheels.

10. Simulation results and analysis thereof

To get an insight into the ESC operation and evaluate its performance, a modeling procedure was elaborated comprising three basic steps:

1) Simulation of a road test with ESC intervention.
2) Simulation of the same road test with the ESC disabled (if simulation results show vehicle skid, the ESC intervention is considered appropriate and efficient).
3) Simulations of the same test with the experimental yawing moment controller enabled.

The third step implies a number of simulations with different settings of the yawing moment controller. Basic parameters to be adjusted are gains P, I and D, which determine "stiffness", accuracy, and response of the regulator. In addition, regulator "dead zone" is adjusted, which specifies controller sensitivity.

Described below is the investigation of a "lane change" maneuver at packed snow, which was performed during the vehicle road testing. Figure 9 shows results of simulations conducted in accordance with steps 1 and 2 of the above-described procedure. Plot colors are explained in legend only briefly, implying the following clarifications:

– "Experiment with ESC" denotes data that were acquired by means of measuring equipment during the road test;

– "Model with ESC" means modeling results simulating the road test (i.e. the first step of the procedure);

– "Model without ESC" corresponds to the modeling with deactivation of the ESC (i.e. the second step of the procedure);

– "wheel11", "wheel12", "wheel21", and "wheel22" denote model variables associated with vehicle wheels (see using ij indices described above).

The plots show following variables (top-down):

– Longitudinal velocity at the vehicle center of gravity ($V_{c.g.,x-v}$): measured during the road test, resulted from the road test simulation, and resulted from the simulation of ESC deactivation.

– Steering wheel angle ($\delta_{s.w.}$) measured during the road test.

– Wheel torques (T_w) identified in simulation of the road test with ESC intervention.

– Vehicle yawing moment (ΣM_{z-v}): resulted from the road test simulation, and from the simulation of ESC deactivation.

– Yaw rate (ω_z): measured during the road test, resulted from the road test simulation, resulted from the simulation of ESC deactivation, and calculated by the single-track vehicle kinematic model (denoted as "Kinem. model").

– Lateral acceleration of the vehicle center of gravity ($a_{y,c.g.}$): measured during the road test, resulted from the road test simulation, and resulted from the simulation of ESC deactivation.

– Wheel sideslip angles (α) calculated during simulation of the road test with ESC intervention.

Model accuracy was estimated by MSEs for three variables, namely, longitudinal velocity of the vehicle, yaw rate, and lateral acceleration at the vehicle center of gravity. Resulted MSEs are shown next to corresponding plots.

From the graphs of identified wheel torques, one can see that ESC exerts the primary (i.e. the largest) correction torque at the front outer wheel, and the secondary torque – at the rear outer wheel. The first ESC intervention is seen in the time interval 6.5…7.2 s (i.e. duration of the intervention was 0.7 s). The major intervention, aimed at prevention of the right skid of the vehicle, took place between 7.2 and 8.3 s (duration of the intervention was 1.1 s). Thus, the full operational cycle of the ESC, beginning with

initiation of the intervention and ending with the vehicle stabilization, in the considered conditions, takes ca. 1 second.

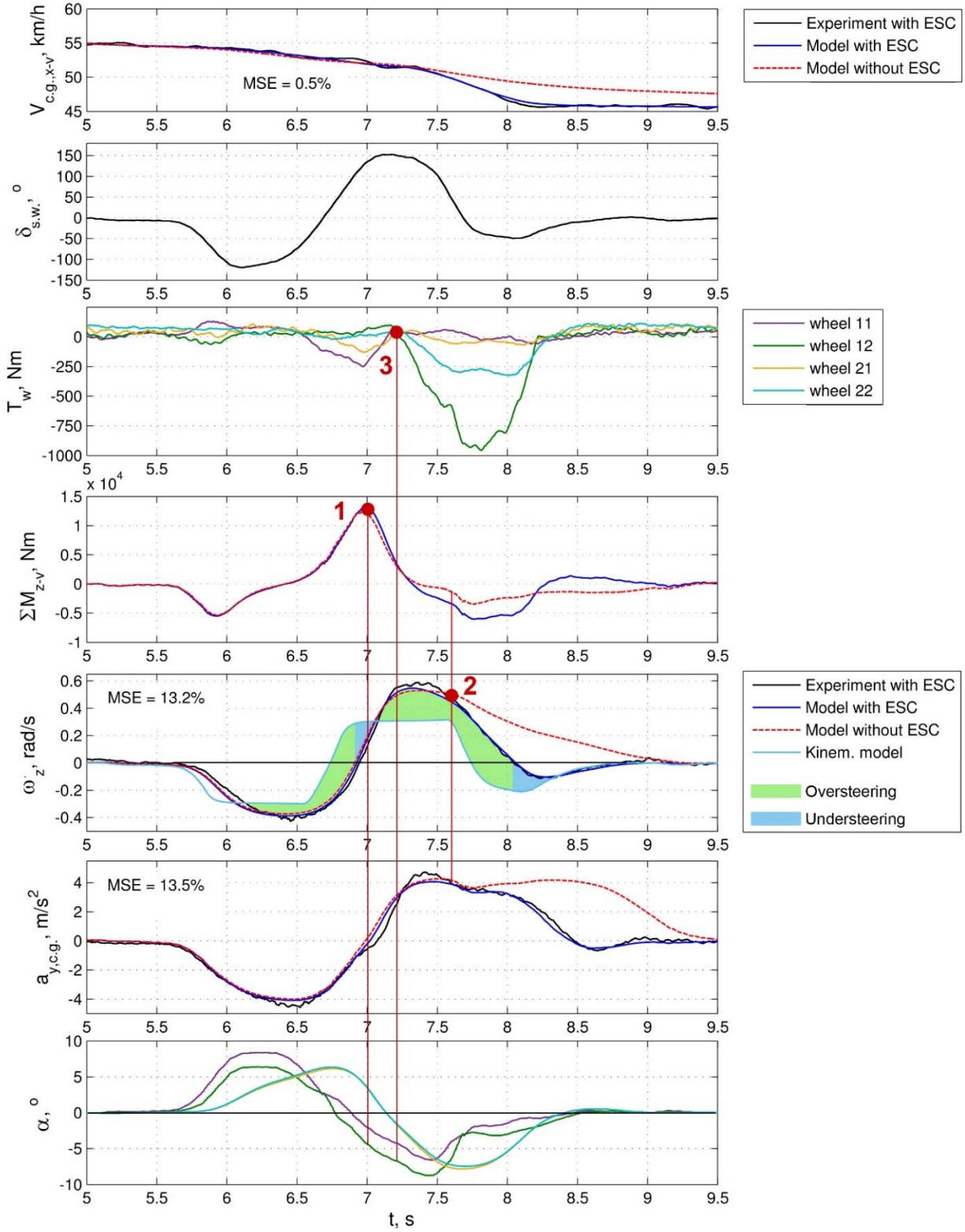

Figure 9. Simulation results: road test with ESC intervention, and results of ESC deactivation ("lane change" maneuver at packed snow).

In figure 9, additional elements are presented intended for the analysis of the vehicle handling characteristics. As it was mentioned previously, the single-track kinematic model corresponds to a vehicle with the neutral steering behavior. Comparing the yaw rate calculated by this model ($\omega_{z,neutral}$) with the actual yaw rate (ω_z), one can evaluate dynamics of the vehicle steering behavior throughout the maneuver. With these quantities having the same sign, expression $|\omega_z| > |\omega_{z,neutral}|$ suggests that vehicle oversteers, while $|\omega_z| < |\omega_{z,neutral}|$ indicates understeering. However, at some stages of the considered maneuver ω_z and $\omega_{z,neutral}$ have opposite signs. For these cases, the following expression can be proposed for defining the steering behavior: $sgn\{(\omega_z - \omega_{z,neutral}) \cdot sgn(\omega_z)\}$. It makes +1 for oversteering and –1 for understeering. Using this expression allowed dividing the maneuver into the stages with different steering behavior. The difference between ω_z and $\omega_{z,neutral}$ is marked by areas of two colors: green for oversteering, and blue for understeering.

Additionally, there are three specific points located on the graphs. Point 1 corresponds to the maximum of yawing moment. It emerges because the rapid counter-steering changes direction of the front tire lateral forces steeply, while the rear lateral forces change their direction with a time lag. As a result, lateral tire forces at the front wheels and the rear wheels, for a certain time, have opposite directions (it can be seen by opposite signs of front and rear sideslip angles), while yawing moments created by these forces become acting in the same direction. The sum of these moments forms a peak, which can be seen at the point 1 of ΣM_{z-a} graph. In the point 2, yaw rates corresponding to the enabled and disabled ESC start to diverge. Therefore, point 2 was assumed an evident beginning of a skid. In the point 3, ESC commences building braking torques, preventing vehicle from the right skid.

It can be concluded that in emergency maneuver, rapid counter-steering entails an excessive yawing moment. Having certain amplitude and duration, this excessive moment brings vehicle into a skid. To prevent this, ESC should intervene at the point located between the maximum of the yawing moment and the beginning of the skid. It can be assumed that in the said point, the process of stability loss has its origin, although no evident signs of a skid are observed. Appearing of known skid indications (rear sideslip angles substantially exceed the front ones) means that rear tire forces provided their maximum ability for counteracting skid, however, the moment exerted by them was insufficient for skid prevention, because excessive yawing moment, emerged previously, has achieved its critical magnitude and duration.

From the simulation results, one can notice specific indications of the stability loss process and their non-consistence with known criteria of the skid:

– The maximum of yawing moment appears when rear tire forces are acting in opposite to the direction of the turn (and of the skid), while rear sideslip angles are diminishing and approaching to zero.

– Stability loss begins (7.15…7.2 s) when rear tire forces and rear sideslip angles are small (in the case at hand, sideslip angles are ca. 1.35^o).

From the aforementioned, it can be concluded that elimination of skid requires ESC intervention to be preventive (i.e. commencing before the skid indications appear), which is actually implemented by the studied production ESC.

Figure 10 shows simulation results for the third step of the procedure (i.e. introducing the experimental yaw rate regulator) along with results of the second step (skid). Graphs are arranged similarly to those in figure 9. Note that in this case, the yaw rate calculated by the kinematic model is also a command signal for the experimental regulator, with $\omega_{z,neutral} - \omega_z$ being the tracking error.

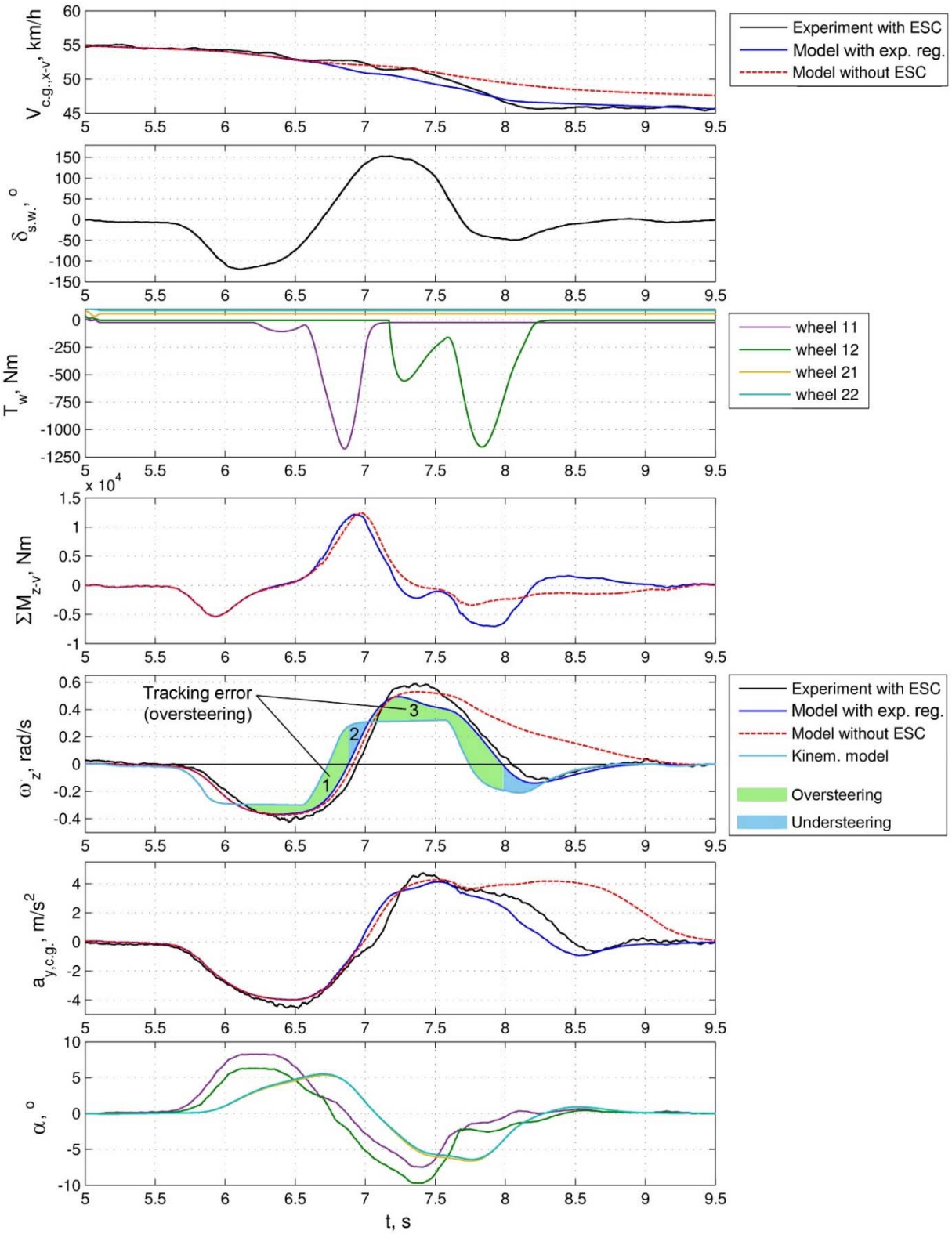

Figure 10. Simulation results: introduction of the experimental regulator, and results of its deactivation ("lane change" maneuver at packed snow).

Graphs show that both intervention time and operating duration of the regulator are similar to those of the production ESC. However, the regulator exerts higher braking torques than the production system, which is due to simplified operation of the former and its "stiffer" adjustments. One can notice that regulator tracking error (oversteering area marked green) is rather large – usually regulators track command signal with higher precision. However, ESC controller should be relatively "soft" due to physical limits of yawing moment correction. A "stiff" controller with higher precision would lock the wheel whatever intensity of the maneuver is; however, the effect of that would hardly be different from, for example, 50…60% braking, since as it is shown by the adhesion characteristics in figure 7, the most significant decrease of lateral adhesion (i.e. the bulk of tire force vector rotation) takes place below 60% slip.

The experimental regulator is only intended for correction of the oversteering. Due to this, transition from the left turn with the oversteering phase (area 1 in figure 10) to the right turn with the short understeering phase (area 2) makes the regulator decrease braking torque at the right wheel (wheel 11) down to zero. The filter at the regulator output does not allow abrupt dropping of the torque, instead bringing it down to zero through a transient process. In the area 3, the right turn with an oversteering phase takes place; therefore, the regulator becomes operating at the left wheel (wheel 12), but not before the torque at the right wheel is reduced to zero.

To verify the assumption about the point 3 (see figure 9) being an origin of the stability loss process, a number of simulations were performed with various presets of the regulator dead zone. It was found that making this dead zone wider weakens initial regulator response in the area 3 (see figure 10) down to the zero torque. As a result, regulator intervention moves in time towards point 2 where the skid takes place. Figure 11 shows the essential variables featuring this experiment, namely the torque at the front left wheel (T_{w12}); vehicle yaw rate (ω_z); vehicle center of gravity coordinates ($X_{c.g.}$, $Y_{c.g.}$) projected on the road plane and thus defining the vehicle trajectory.

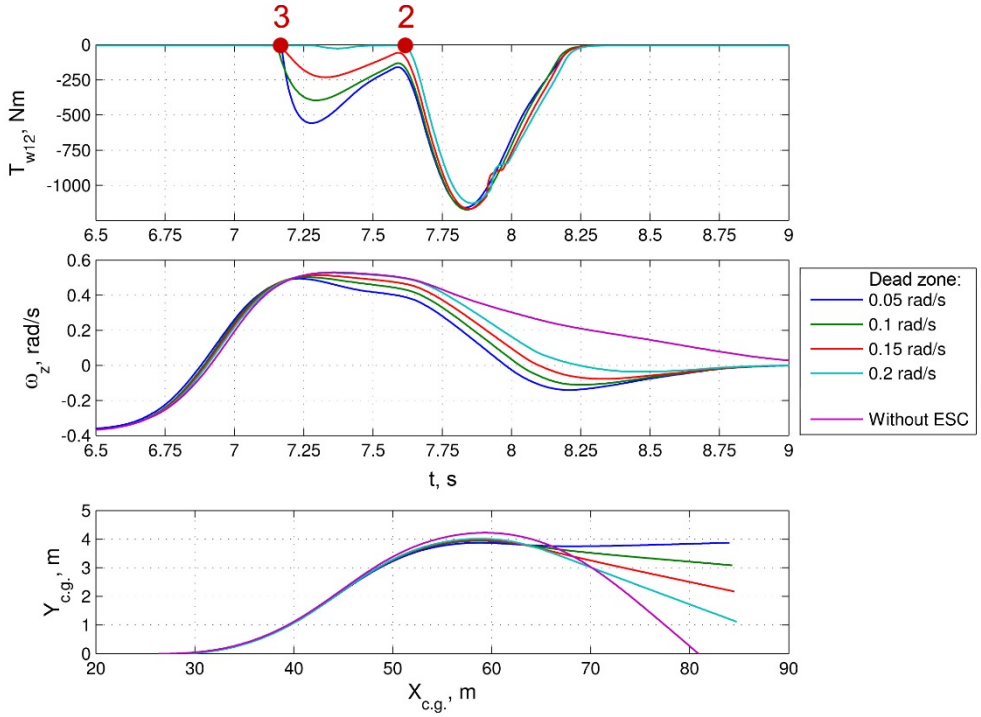

Figure 11. Influence of the yaw rate regulator dead zone on the vehicle directional stability.

Presented graphs show that weakening of the initial regulator response (dead zone > 0.05 rad/s) results in increased oversteering. With dead zone 0.2 rad/s, the regulator intervened after skid indications have appeared (from 7.6 seconds on), and after that, even exerting of an appropriate correcting torque

has not prevented the vehicle from the loss of stability. Therefore, conducted simulations verified that ESC operates effectively when it intervenes at the beginning of the stability loss process. The latter can be recognized from the difference between the required and the actual yaw rate, rather than from known indications of the skid (i.e. large rear sideslip angles and the maximum adhesion seen at the rear wheels). It was shown that the production ESC provides such preventive intervention, as well as the experimental regulator having dead zone 0.05 rad/s.

Figure 12 shows vehicle trajectories resulted from each step of the above-described research procedure. Trajectory of the vehicle with the experimental regulator was obtained with the dead zone 0.05 rad/s. Intervention of the experimental regulator resulted in a lower vehicle lateral accelerations than those obtained with the production ESC. This prevented vehicle from excessive drifting towards the margin of the left lane (however, this should not be considered as some advantage of the experimental regulator over the production system, but rather a mere observation made from the simulations).

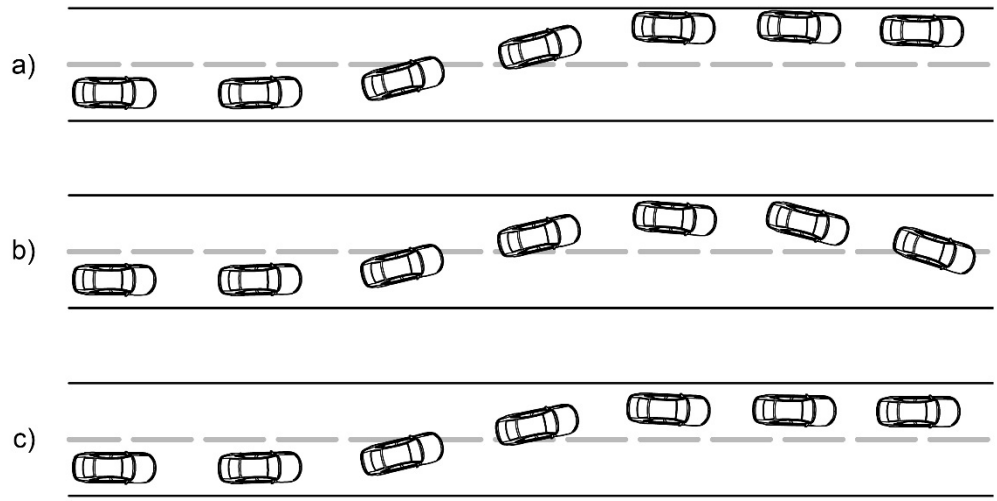

Figure 12. Vehicle trajectories obtained in simulations. a – road test simulation with ESC intervention, b – disabling of the ESC, c – with the experimental regulator.

Studies similar to the described in this article were conducted for a number of maneuvers at different vehicle speeds, both at snow and ice, with the results alike. In most experiments, MSEs of the following orders were obtained: 10…20% for both lateral acceleration and yaw rate, at most 12% for the longitudinal acceleration, and at most 2% for the longitudinal velocity. Based on literature analysis on vehicle dynamics modeling, and also considering non-rigidity (to a certain extent) of the snow surface as well as involvement of studded tires (which adhesion characteristics are known to be rather scattered [15]), obtained MSEs were considered proving a sufficient accuracy of the model.

11. Conclusions

Elaborated model of vehicle dynamics allows simulation of vehicle tests at snow-covered surfaces with sufficient accuracy substantiated by reasonable relative mean square errors. The method employed for identification of unmeasured wheel torques allowed disclosing the ESC interventions occurred during the road test. Identification results were validated indirectly, i.e. by MSEs of the essential vehicle dynamic parameters, and by comparing identified interventions with descriptions given in the literature by the ESC producers (e.g. Bosch).

Proposed 3-step modeling procedure allowed to discover that at snow-covered surfaces both production ESC and the experimental regulator prevent the vehicle from the loss of directional stability. Disabling the ESC or said regulator brings vehicle into a skid seen from its trajectory and specific changes in yaw rate and lateral acceleration.

Analysis of the simulation results revealed stages of the emergency maneuver associated with directional stability (whether it is maintained or lost). Three specific points can be distinguished. The first one corresponds to the maximum yawing moment resulted from opposite directions of front and rear lateral tire forces. The second point indicates the beginning of a skid, which can be recognized either by a substantial growth of rear sideslip angles or by distinctive increase in yaw rate and lateral acceleration. In the third point, temporally located between the first one and the second one, the ESC should intervene to prevent vehicle from a skid. In this point, lateral tire forces (or sideslip angles) of the rear wheels are close to zero. Time locations of said points suggest that ESC should intervene preventively, i.e. when stability loss originates, not when it reveals itself. Analysis of the modeling results showed that both production ESC and the experimental regulator satisfy this requirement.

Skid prevention effectiveness depends on adjustments of the yaw rate controller, in particular its dead zone. Conducted study has shown that the experimental regulator possessed the effectiveness comparable to that of the production ESC, when the dead zone was ca. 0.05 rad/s. Increasing of this threshold brings the point of regulator intervention closer to the beginning of the skid deteriorating the system performance.

Appendix. Nomenclature of variables and parameters

Variable/parameter designation	Variable/parameter name	Value and/or dimension
a_1, a_2	vehicle front and rear tracks	1.6, 1.66 m
$a_{x,c.g.}$, $a_{y,c.g.}$	components of the vehicle center of gravity acceleration vector projected on vehicle axes	m/s^2
b	vehicle wheel base	3.07 m
b_1, b_2	longitudinal distance from the vehicle center of gravity to the centers of front and rear axles respectively	1.5, 1.57 m
c_φ	suspension roll stiffness	N·m/rad
d_φ	suspension roll damping coefficient	N·m/rad/s
e_ω	yaw rate controller tracking error	rad/s
$F_{w,x}$, $F_{w,y}$	components of the air drag force vector projected on the vehicle axes	N
g	gravity constant	9.81 m/s^2
G_{xy}, G_{yx}	correction functions for longitudinal and lateral tire forces taking into account combined slip (MF model)	–
h_{ij}	tire force arm	m
$h_{c.g.}$	vehicle center of gravity height	0.639 m
$\mathcal{J}_w$	wheel inertia	1.62 kg·m^2
$\mathcal{J}_{x,sprung}$	roll inertia of the sprung mass	920 kg·m^2
$\mathcal{J}_z$	vehicle yaw inertia	5500 kg·m^2
k	number of wheels (tires) at *i*-th axis	2
m	vehicle mass	2558 kg
M_{z-v}	yawing moment exerted by the wheel	N·m
M_{z-w}	tire aligning moment	N·m
n	number of vehicle axes	2
r	wheel radius	m
r_e	wheel rolling radius	m
r_{e0}	effective rolling radius	m
R	turning radius of the rear axle center	m
R_{ij}	tire force	N
R_{y-v}, R_{x-v}	components of the tire force vector projected on the vehicle axes	N

R_{x-w}, R_{y-w}	components of the tire force vector projected on the wheel axes	N
R_z	tire normal force	N
S_x	tire longitudinal slip	–
T_w	wheel torque	N·m
$V_{c.g.,x-v}$, $V_{c.g.,y-v}$	components of the vehicle center of gravity velocity vector projected on the vehicle axes	m/s (km/h for plots)
V_w	linear velocity of the wheel center	m/s
$V_{w,x-v}$, $V_{w,y-v}$	components of the wheel center velocity vector projected on the vehicle axes	m/s
u_{steer}	vehicle steering ratio	–
u	control signal	–
$X_{c.g}$, $Y_{c.g}$	vehicle center of gravity coordinates projected on the road plane	m
y_{w-v}	lateral displacement of the wheel with respect to the vehicle axes	m
α	sideslip angle of the wheel	rad (^{o} for plots)
$\delta_{s.w.}$	steering wheel angle	rad (^{o} for plots)
δ	steer angle of the wheel	rad
ΔM_z	correcting yawing moment	N·m
μ_x, μ_y	longitudinal and lateral tire-surface adhesion coefficients	–
φ	roll angle	rad
ψ_z	yaw angle	rad
ω_w	wheel angular speed	rad/s
ω_z	yaw rate	rad/s
ω_z *	yaw rate command	rad/s
$\omega_{z,neutral}$	yaw rate calculated by the single-track model with rigid wheels	rad/s

References

[1] Ivanov A M Kristalnyi S R Popov N V and Fomichev V A 2018 Results of tests of the vehicle ESP system efficiency equipped with studded tires (in Russian) *Journal of Automotive Engineers* (Russia) **2** (109) pp 40-44

[2] Fomichev V A 2017 *A method for performance assessment of electronic stability control systems for vehicles equipped with studded tires* PhD thesis (Russian)

[3] Wiessalla J Mao Y and Esser F 2015 *From Tyre Measurements on Low μ Surface to Full Vehicle ESC Simulations under Winter Conditions*. Proc. of the 4th Int. Tyre Colloquium pp 324-329

[4] Liebemann E K Meder K Schuh J and Nenninger G. 2005 *Safety and Performance Enhancement: The Bosch Electronic Stability Control (ESP)*. 19th Int. Technical Conf. on the Enhanced Safety of Vehicles (ESV)

[5] Isermann R (Hrsg.) 2006 *Fahrdynamik-Regelung. Modellbildung, Fahrerassistenzsysteme, Mechatronik* (Friedr. Vieweg & Sohn Verlag | GWV Fachverlage GmbH, Wiesbaden) pp 169-211

[6] Lata V N 1989 *Selection and investigation of vehicle handling ability criteria by means of frequency analysis* PhD thesis (Russian)

[7] Goggia T Sorniotti A De Novellis L Ferrara A Pennycott A Gruber P and Yunus I 2015 Integral sliding mode for the yaw moment control of four-wheel-drive fully electric vehicles with in-wheel motors *Int. Journal of Powertrains* **4** pp 388-419

[8] Pandit C A *Model-free Approach to Vehicle Stability Control* 2013 PhD Thesis

[9] Zang H, Zhang S Dai Y and Congna D 2017 The Research of Vehicle Handling Performance and Stability Based on the Integrated Control of Electronic Stability Program and Anti-block

Braking System *Boletín Técnico* **55** pp 634-640
[10] Du H Zhang N and Smith W 2009 Robust Yaw Moment Control for Vehicle Handling and Stability *SAE Technical Papers* **2009-01-0578**
[11] Mirzoev G K and Peshkilev A G 1980 Computer Analysis of Suspension Kinematics (in Russian) *Automotive Industry* (Russia) **2** 12-14
[12] Pacejka H B and Besselink I 2012 Tire and vehicle dynamics. Third Edition (Elsevier Ltd.) pp 165-183
[13] Kulikov I A Bakhmutov S V and Barashkov A A 2016 An Investigation of Vehicle Dynamics Concerning Active Safety Systems by Simulations and Driving Tests *Proc. of NAMI* **265** pp 53-65
[14] Kulikov I A 2016 Advanced Tools for Research and Development of Hybrid Vehicles Based on the Component-in-the-Loop Technology PhD thesis (Russian Federation) pp 65-71
[15] Svendenius J 2007 *Tire Modeling and Friction Estimation* Lund University pp 130-133